Proton ENDOR Spectroscopy of Bis(2,2,6,6-tetramethylheptane-3,5-dionato)-copper(II) and Crystal Structure of Bis(2,2,6,6-tetramethylheptane-3,5-dionato)-palladium(II) †

Gareth J. Baker and J. Barrie Raynor *
Department of Chemistry, The University, Leicester LE1 7RH
Jan M. M. Smits and Paul T. Beurskens
Department of Crystallography, University of Nijmegen, Toernooiveld, 6525 ED Nijmegen, The Netherlands
Huub Vergoossen and C. (Kees) P. Keijzers
Department of Molecular Spectroscopy, University of Nijmegen, Toernooiveld, 6525 ED Nijmegen, The Netherlands

The proton electron nuclear double resonance spectroscopy of a single crystal of bis(2,2,6,6-tetramethylheptane-3,5-dionato)copper(II) in the palladium analogue has been studied. Tensors could be determined for the γ-proton and two nearest Bu^t protons as well as six protons on the nearest-neighbour palladium complex. The assignment of most of these was enabled by the comparison with theoretically calculated tensors. This calculation procedure has been described previously: it uses the molecular orbital coefficients as obtained from an extended Hückel calculation and includes all two- and three-centre contributions. The remaining experimental curves could not be fitted to calculated tensors. The structure of the palladium analogue, $C_{22}H_{38}O_4Pd$, was determined by *X*-ray crystallography at 140 K: monoclinic, space group $P2_1/n$, a = 11.245(3), b = 12.008(8), c = 9.851(3) Å, β = 110.17(3)°, and Z = 2 (Mo-K_α radiation, graphite crystal monochromator). Final conventional R = 0.029, R' = 0.044 for 1 654 unique reflections and 186 variables.

As part of a detailed e.s.r. and electron nuclear double resonance (ENDOR) spectroscopic study of the structure and bonding in complexes involving the acetylacetonate class of chelating ligands, we have made measurements on single crystals of [Cu(tmhd)$_2$] doped into the corresponding diamagnetic palladium analogue (tmhd = 2,2,6,6-tetramethylheptane-3,5-dionate, pd = pentane-2,4-dionate = acetylacetonate). The most suitable diamagnetic host lattices for Cu^{II} are the corresponding Pd^{II} complexes. However, of the Pd^{II} complexes with the acetylacetonate class of chelating ligands, [Pd(R^{1}COCHCOR^2)$_2$], crystal structure determinations have been carried out only for R^1 = R^2 = Me;[1] R^1 = Ph, R^2 = Pr^n;[2] R^1 = Ph, R^2 = Me;[3] and R^1 = CF$_3$, R^2 = Bu^t.[4] Our host complex, [Pd(tmhd)$_2$], has R^1 = R^2 = Bu^t and as such there is a possibility of disorder arising from different orientations of the methyl groups at room temperature. To reduce this possibility and in order to obtain accurate proton positions, the crystal structure was determined at 138 ± 4 K.

Crystal structures are known for the analogous copper complexes [Cu(R^{1}COCHCOR^2)$_2$] where R^1 = R^2 = Me;[5] R^1 = Ph, R^2 = Me;[6] R^1 = R^2 = Ph;[7] and R^1 = R^2 = Bu^t.[8] In the case of R^1 = R^2 = Me and R^1 = Ph, R^2 = Me where the structures of both the Cu and Pd complexes are known, the pairs of complexes are isomorphous.

Single-crystal e.s.r. measurements have only been carried out on [Cu,Pd(pd)$_2$],[9–11] [Cu,Pd(PhCOCHCOMe)$_2$],[11] and [Cu,Ni(Bu^{t}COCHCOBu^t)$_2$][12,13] from which considerable information has been deduced about the bonding in these complexes. The only proton ENDOR study on the acetylacetone class of Cu complexes has been by Kirste and van Willigen[14] on frozen solutions of [Cu(pd)$_2$]. Our work on [Cu,Pd(tmhd)$_2$] is new and more definitive than studies on related molecules of this class, and is coupled with extended Hückel molecular orbital (EHMO) calculations and elaborate computations of proton hyperfine coupling tensors, which include two- and three-centre contributions.

Experimental

The complex [Pd(tmhd)$_2$] was prepared by the method of Okeya *et al.*[3] and recrystallised from a CH_2Cl_2–toluene mixture. Doped single crystals of [Pd(tmhd)$_2$] with *ca.* 1% Cu were grown from CH_2Cl_2–toluene by slow evaporation. The [Cu(tmhd)$_2$] was prepared by standard methods. ENDOR spectra were recorded on a Varian E12 e.s.r. spectrometer with a Varian E1737 ENDOR cavity as described previously.[15] The ENDOR spectra were recorded in three approximately orthogonal but arbitrary planes at 25 K using an Oxford Instruments BKESR12 flow cryostat. Because of the complexity of the spectra and the rotation patterns, both e.s.r. and ENDOR spectra were measured every 4°. The co-ordinate system and numbering scheme for the molecule are shown in Figure 1. At each angle, the frequency and magnetic field were measured using a Hewlett Packard 5246L counter with a 5255A plug-in unit and a Bruker B-NM12 gaussmeter respectively.

X-Ray Structure Determination.—All measurements were made at T = 140 K. Crystals, doped with 1 mol % Cu, had to be cut to obtain fragments of suitable size. An irregularly shaped fragment *ca.* 0.15 × 0.20 × 0.20 mm was used for all measurements. This irregular shape, together with the necessity to put the crystal in a glass capillary in a cold nitrogen gas stream, prevented the application of an analytical absorption correction. Throughout the experiment Mo-K_α radiation was used with a graphite-crystal monochromator on a Nonius CAD4 single-crystal diffractometer (λ = 0.709 26 Å).

Crystal data. The unit-cell dimensions, a = 11.245(3), b = 12.008(8), c = 9.851(3) Å, β = 110.17(3)°, U = 1 248.6 Å^3, were determined from the angular settings of 25 reflections with

† *Supplementary data available* (No. SUP 56639, 4 pp.): H-atom co-ordinates, thermal parameters. See Instructions for Authors, *J. Chem. Soc., Dalton Trans.*, 1986, Issue 1, pp. xvii—xx.

Table 1. Final fractional co-ordinates and isotropic thermal parameters ($Å^2$) with e.s.d.s in parentheses and site occupancy factors, if not one

Atom	x	y	z	10^2U_{eq}	S.o.f.
Pd(1)	0.0	0.0	0.0	3.52(1)	
O(1)	0.105 47(23)	−0.017 19(16)	−0.121 63(25)	4.57(9)	
C(1)	0.205 7(3)	0.039 80(26)	−0.106 7(3)	3.87(10)	
C(2)	0.257 3(3)	0.118 66(26)	0.000 2(3)	4.35(11)	
C(3)	0.210 6(3)	0.151 74(23)	0.108 0(3)	3.86(10)	
O(2)	0.111 44(19)	0.114 47(17)	0.124 76(21)	4.48(8)	
C(4)	0.262 2(3)	0.011 85(27)	−0.222 7(4)	4.73(12)	
C(5)	0.164 2(5)	0.043 8(5)	−0.368 2(5)	7.61(19)	
C(6)	0.287 6(5)	−0.112 9(4)	−0.216 0(6)	7.57(22)	
C(7)	0.385 0(4)	0.073 2(4)	−0.205 8(5)	6.78(18)	
C(8)	0.278 9(3)	0.239 9(3)	0.220 3(4)	5.03(13)	
C(9)	0.343 7(10)	0.181 3(8)	0.361 3(10)	7.19(24)	0.50
C(10)	0.389 3(7)	0.299 2(7)	0.181 8(8)	4.89(17)	0.50
C(11)	0.188 1(10)	0.324 0(9)	0.233 2(13)	7.85(28)	0.50
C(9A)	0.406 9(18)	0.180 8(15)	0.328 6(21)	7.24(27)	0.25
C(10A)	0.318 8(19)	0.339 7(15)	0.159 9(19)	7.24(27)	0.25
C(11A)	0.205 1(17)	0.269 0(16)	0.326 0(20)	7.24(27)	0.25
C(9B)	0.280 6(15)	0.210 8(12)	0.365 8(16)	4.74(19)	0.25
C(10B)	0.419 2(13)	0.258 5(13)	0.229 2(16)	4.74(19)	0.25
C(11B)	0.195 4(14)	0.349 3(13)	0.172 8(17)	4.74(19)	0.25

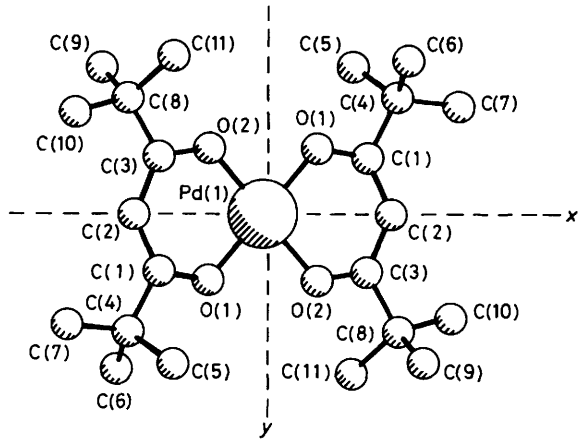

Figure 1. Numbering scheme of atoms in $[Pd(tmhd)_2]$

$13 < \theta < 17°$. The space group was determined to be $P2_1/n$ from the systematic absences $0k0: k = 2n + 1$ and $h0l: h + l = 2n + 1$ and the structure determination.

Data collection. The intensity data of 8 802 reflections (the full sphere up to $\theta = 30°$) were measured, using the ω—2θ scan technique, with a scan angle of 1.50° and a variable scan rate with a maximum scan time of 30 s per reflection. The intensity of the primary beam was checked throughout the data collection by monitoring three standard reflections every 30 min. The final drift correction factors were between 1.00 and 1.12. Profile analysis was performed on all reflections.[16,17] Empirical absorption correction was applied, using ψ-scans,[18] $\mu(Mo\text{-}K_\alpha) = 15.09\ cm^{-1}$ (correction factors were in the range 0.94—1.00). Lorentz and polarisation corrections were applied and the data were reduced to $|F_o|$ values. Laue symmetry-equivalent reflections were averaged, $R_{int.} = \Sigma(F - \langle F \rangle)/\Sigma F = 0.035$ for all reflections and 0.011 for the observed reflections only, resulting in 2 203 unique reflections of which 1 678 were observed with $F > 3\sigma(F)$.

Determination and refinement of the structure. Since the palladium atom must lie on a special position, it was placed in the origin and used as input for DIRDIF,[19] which gave all non-hydrogen atoms. During the refinement process it became clear that one of the two tertiary butyl groups of the unique part of the molecule could not be described adequately in the usual way. The thermal parameter of the three methyl groups involved were much too high, so three Me_3 groups, with occupancy factors of 0.50, 0.25, and 0.25 (based on Fourier peak heights), were introduced, allowing for mainly rotational disorder. Of the nine CH_3 positions involved, the carbon atoms labelled C(9), C(10), and C(11) form methyl groups with occupancy factor 0.50 and three individual isotropic thermal parameter. The carbon atoms labelled C(9A), C(10A), and C(11A) form a group with occupancy factor of 0.25 and one common isotropic thermal parameter; the same holds for the third group with the carbon atoms labelled C(9B), C(10B), and C(11B). All groups had fixed, idealised hydrogen atoms attached to the carbon atoms. All other hydrogen atoms were located in a difference Fourier synthesis, and included in the refinement.

Isotropic least-squares refinement using SHELX[20] converged to $R = 0.054$. At this stage an empirical absorption correction was applied,[21] resulting in a further decrease of R to 0.050. Relative absorption correction factors were in the range 0.897—1.064.

During the final stages of the refinement all positional parameters were refined, treating the disordered CH_3 groups as rigid groups. The thermal parameter of the disordered groups were refined isotropically, as indicated above. Apart from these groups, all other non-hydrogen atoms were given anisotropic thermal parameter and the hydrogen atoms fixed isotropic thermal parameter of 0.07 $Å^2$.

The final conventional agreement factors were $R = 0.029$ and $R' = 0.044$ for 1 654 'observed' reflections and 186 variables. The function minimized was $\Sigma w(F_o - F_c)^2$ with $w = 1/[\sigma^2(F_o) + 0.0005\ F_o^2]$ with $\sigma(F_o)$ from counting statistics. The maximum shift/error ratio in the last full-matrix least-squares cycle was <0.06 for the non-disordered part of the molecule and <0.5 for the disordered part. The final difference Fourier map showed no peaks >0.5 e $Å^{-3}$.

The scattering factors used were from International Tables.[22] No correction was made for the presence of 1% copper.

Results and Discussion

Crystal Structure.—Final positional and thermal parameters are given in Table 1; molecular geometry data are collected in Tables 2—4. Drawings of the molecule in minimum overlap position, showing the molecular configuration, are given in Figures 2 and 3.

As one of the aims of the structure determination was to determine the interaction between the palladium atom and the surrounding hydrogen atoms, much emphasis was placed on the determination of the geometry of the disordered trimethyl groups. The data for the geometry of the disordered groups are collected. The C–H bond distances and H–C–H angles were fixed. The isotropic thermal parameter of the three Me groups with occupancy factor of 0.50 were refined to 0.072, 0.048, and 0.079 $Å^2$ respectively. The isotropic thermal parameter of the two trimethyl groups refined to 0.073 and 0.048 $Å^2$. All these values indicate reasonable geometries, and the proposed structure accounts well for the observed structure factors. The three trimethyl groups are not evenly separated in space; this could indicate that the rotational freedom that is present is constrained by interactions between hydrogen atoms and the palladium atom.

E.S.R. Spectra.—A typical spectrum at a random orientation is shown in Figure 4. It shows the copper sites and the isotope splitting. The e.s.r. data at 25 K were analysed using the ESR64

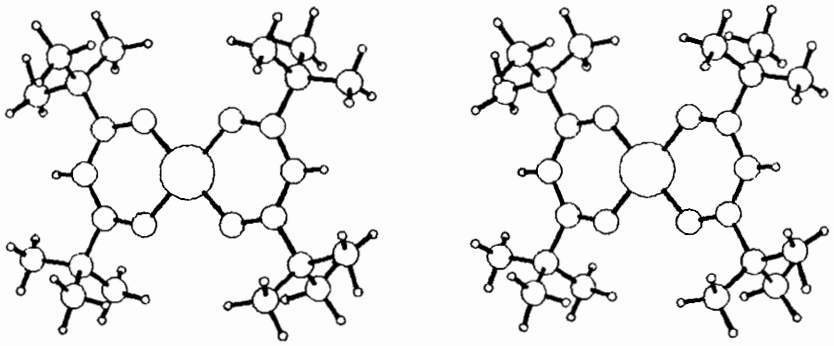

Figure 2. Stereoview of the $[Pd(tmhd)_2]$ molecule in minimum overlap projection, including hydrogen atoms

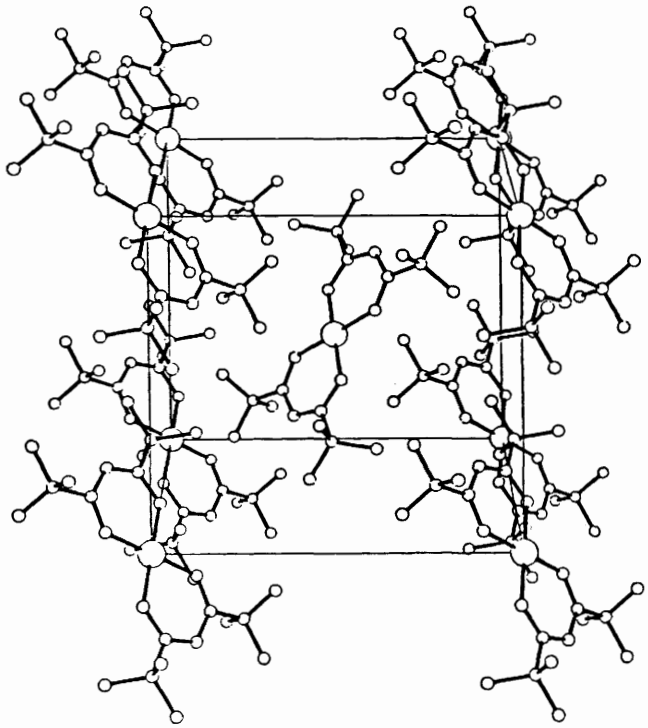

Figure 3. Two molecules of $[Pd(tmhd)_2]$, including hydrogen atoms in minimum overlap projection

program which diagonalises the Hamiltonian matrix. ESR64 is a function subroutine of a minimization program and minimizes the error function (1) by varying (in this application*)

$$h\left[\frac{1}{N}\sum_{i=1}^{N}(\nu^{i}_{obs.}-\nu^{i}_{calc.})^2\right]^{\frac{1}{2}} \qquad (1)$$

the elements of the g tensor and the copper hyperfine and quadrupole interaction tensors. In the analysis of e.s.r. data, ν is the microwave frequency; in the analysis of ENDOR spectra (see below) it is the radio frequency. The summation runs over all e.s.r. (or ENDOR) transitions in all spectra which are measured in the three planes.

In this way, the $\bar{\bar{g}}$, $\bar{\bar{A}}^{Cu}$, and $\bar{\bar{P}}^{Cu}$ tensors were obtained in the laboratory system (l.s.) for both magnetically inequivalent molecules in the unit cell. Since the measurements were performed in three *arbitrary* planes, transformation of the principal axes from the l.s. to the molecular co-ordinate system (m.c.s.) was only possible in the following way: the crystallographic b axis could be located in the l.s. because it must be a symmetry axis between the tensors of the two sites. A second axis could be found by *assuming* that $g_{\|}$ and $A_{\|}$ are along the molecular z axis. A check showed that the angle between the b axis and $g_{\|}$, $A_{\|}$ (being half the angle between the $g_{\|}$ vectors of the two sites) is indeed within one degree equal to the angle between the b axis and the z axis. The resulting principal values and axes of

* For other applications of the program ESR64, see, for example, M. L. H. Paulissen and C. P. Keijzers, *J. Mol. Struct.*, 1984, **113**, 267.

Table 2. Bond lengths (Å) with e.s.d.s in parentheses for the non-disordered part of the molecule

Pd(1)–O(1)	1.966(2)	C(3)–O(2)	1.265(3)
Pd(1)–O(2)	1.977(2)	C(3)–C(8)	1.534(4)
O(1)–C(1)	1.284(4)	C(4)–C(5)	1.526(6)
C(1)–C(2)	1.387(4)	C(4)–C(6)	1.524(5)
C(1)–C(4)	1.525(5)	C(4)–C(7)	1.523(5)
C(2)–C(3)	1.395(4)		

Table 3. Bond angles (°) with e.s.d.s in parentheses for the ordered part of the molecule

O(1)–Pd(1)–O(2)	93.8(1)	O(2)–C(3)–C(8)	113.3(3)
Pd(1)–O(1)–C(1)	124.4(2)	Pd(1)–O(2)–C(3)	124.3(2)
O(1)–C(1)–C(2)	125.0(3)	C(1)–C(4)–C(5)	107.1(3)
O(1)–C(1)–C(4)	111.9(3)	C(1)–C(4)–C(6)	107.7(3)
C(2)–C(1)–C(4)	123.1(3)	C(5)–C(4)–C(6)	110.6(4)
C(1)–C(2)–C(3)	127.2(3)	C(1)–C(4)–C(7)	114.1(3)
C(2)–C(3)–O(2)	125.4(3)	C(5)–C(4)–C(7)	108.4(4)
C(2)–C(3)–C(8)	121.3(3)	C(6)–C(4)–C(7)	108.8(3)

Table 4. Bond lengths (Å) and angles (°) with e.s.d.s in parentheses for the disordered part of the molecule

C(8)–C(9)	1.503(10)	C(8)–C(9A)	1.630(18)	C(8)–C(9B)	1.468(14)
C(8)–C(10)	1.587(8)	C(8)–C(10A)	1.476(17)	C(8)–C(10B)	1.566(14)
C(8)–C(11)	1.474(10)	C(8)–C(11A)	1.579(18)	C(8)–C(11B)	1.591(15)

C(3)–C(8)–C(9)	107.8(4)	C(9A)–C(8)–C(10A)	107.2(10)
C(3)–C(8)–C(10)	112.1(4)	C(9A)–C(8)–C(11A)	102.2(10)
C(3)–C(8)–C(11)	110.3(5)	C(10A)–C(8)–C(11A)	112.8(11)
C(9)–C(8)–C(10)	105.1(5)	C(3)–C(8)–C(9B)	112.0(6)
C(9)–C(8)–C(11)	111.8(7)	C(3)–C(8)–C(10B)	112.6(6)
C(10)–C(8)–C(11)	109.6(6)	C(3)–C(8)–C(11B)	105.1(6)
C(3)–C(8)–C(9A)	106.3(7)	C(9B)–C(8)–C(10B)	107.8(9)
C(3)–C(8)–C(10A)	114.7(7)	C(9B)–C(8)–C(11B)	107.0(9)
C(3)–C(8)–C(11A)	112.5(8)	C(10B)–C(8)–C(11B)	112.4(8)

Table 5. Experimental and calculated principal values and axes (relative to the molecular axis system) of the $\bar{\bar{g}}$, $\bar{\bar{A}}^{Cu}$, and $\bar{\bar{P}}^{Cu}$ tensors for the $[Cu^{II}(tmhd)_2]$ complex in the Pd^{II} host. $\bar{\bar{A}}^{Cu}$ and $\bar{\bar{P}}^{Cu}$ are in units of 10^{-4} cm^{-1}. Experimental directions are accurate to $\pm 5°$

	Experimental				Calculated			
		x	*y*	*z*		*x*	*y*	*z*
g_1	2.244	90	90	1	2.220	90	88	2
g_2	2.053	44	45	89	2.056	97	7	92
g_3	2.049	134	45	90	2.055	7	83	90
A_1	−110.5	90	89	1	−102.6	90	88	2
A_2	52.0	81	8	90	50.8	88	2	92
A_3	58.5	9	98	89	51.8	2	88	90
A_{iso}*	−82.6							
P_1	2.0	98	89	9	5.4	90	88	2
P_2	0.2	37	53	83	−3.1	91	2	92
P_3	−2.2	55	143	84	−2.3	1	89	90

* Because of spin polarisation, A_{iso} cannot be computed from EHMO calculations.

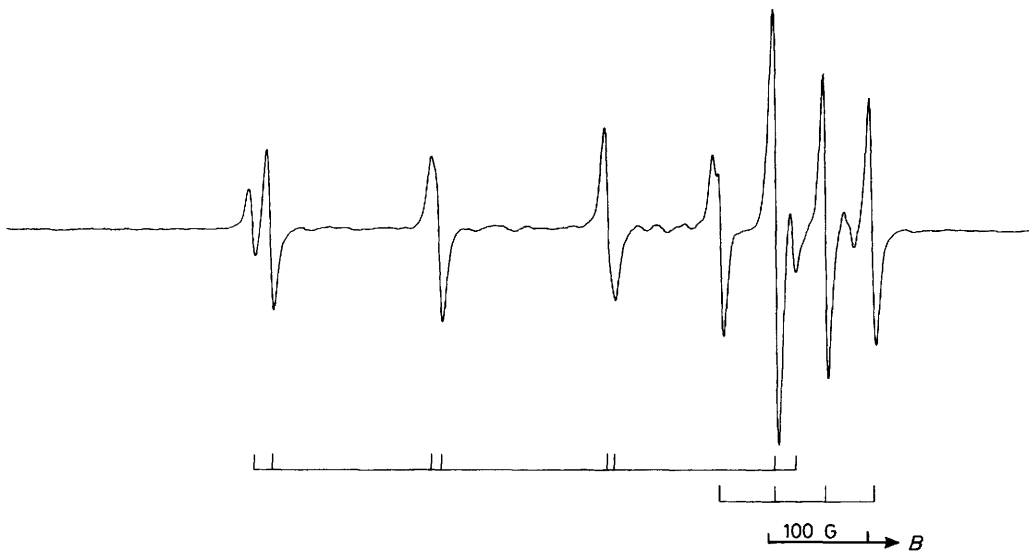

Figure 4. Typical e.s.r. spectrum of $[Cu,Pd(tmhd)_2]$ at random orientation showing the two sites in the lattice (G = 10^{-4} T)

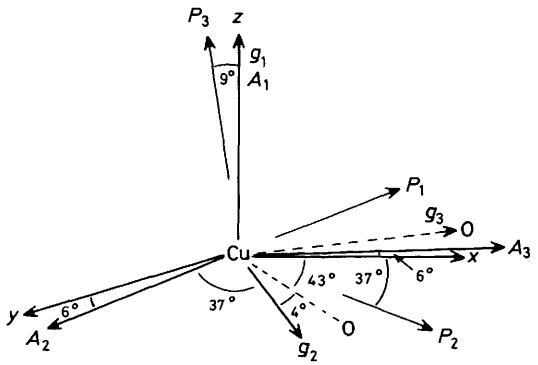

Figure 5. Orientation of the $\bar{\bar{g}}$ and $\bar{\bar{A}}^{Cu}$ tensors relative to the molecular axis system for $[Cu(tmhd)_2]$. The *x* axis bisects the chelate O–Cu–O angle (86°)

the *g* tensor and the Cu hyperfine- and quadrupole-interaction tensors are listed in Table 5. Their orientation relative to the molecular axis system is shown in Figure 5. The principal directions of $\bar{\bar{g}}$ and $\bar{\bar{A}}^{Cu}$ coincide with the molecular *z* axis. The other *g* directions are not along the molecular symmetry axes, but along the direction of one of the Cu–O bonds. The principal directions of the hyperfine tensor lie close to the molecular symmetry axes as expected. The very small *g* anisotropy in the *xy* plane means that small changes to the off-diagonal elements by symmetry lowering, or small experimental errors, can cause quite large rotations of the principal directions in this plane. The *g* tensor and $\bar{\bar{A}}^{Cu}$ agree very well with experimental observations on similar systems.[10,12] Also the tensors which are obtained from the EHMO data (in a manner similar to ref. 23), which are also listed in Table 5, agree well with the experimental results. The only exception is the quadrupole tensor. The calculated tensor contains only one-centre contributions and is, therefore, very inaccurate. The experimental tensor is inaccurate also, because it is determined by small second-order shifts of the spectral lines. It is satisfying, however, that experimentally as well as theoretically the largest positive principal value is directed along the *z* axis, perpendicular to the molecular plane. The most accurate of all experimental determinations of this tensor[9-11,24] was that of Kita *et al.*,[10] who applied ^{63}Cu ENDOR. Their result was $P_1 = -0.71 \times 10^{-4}$, $P_2 = -1.61 \times 10^{-4}$, $P_3 = +2.31 \times 10^{-4}$ cm^{-1},

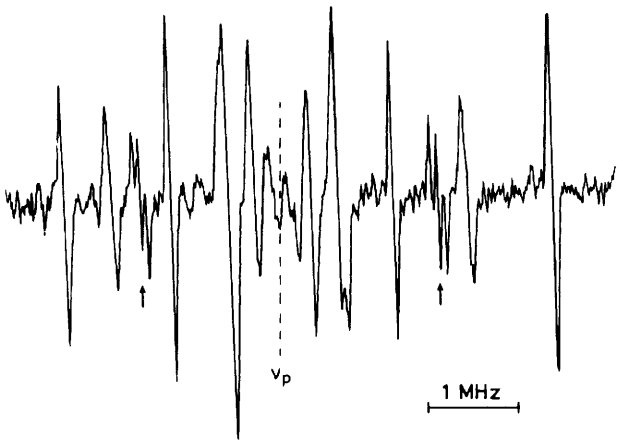

Figure 6. Typical ENDOR spectrum from a single crystal of [Cu,Pd(tmhd)$_2$] showing triplet splitting (↑) of some of the lines due to proton–proton interactions

ca. 50% of our calculated tensor. The *g* tensor was calculated earlier by Cotton *et al.*[13] also from EHMO data. Their result agrees well with ours.

ENDOR Spectra.—A typical spectrum is shown in Figure 6. The linewidths are of the order of 25 kHz; the accuracy of the measured transition frequencies is within *ca.* 5 kHz. The angular variation of the ENDOR frequencies in one of the three measured planes is shown in Figure 7; here the experimental frequencies have been scaled to a free proton frequency of 13 MHz. The complexity of the spectra is caused by the fact that each molecule has 19 symmetry-unrelated protons, giving rise to 38 ENDOR lines. This number is increased by the hyperfine interaction with protons of neighbouring molecules, directly through space instead of through delocalisation of the unpaired electron.

The ENDOR data were analysed for each proton individually, with the spin-Hamiltonian (2). In this Hamiltonian,

$$\mathcal{H} = \mu_B \vec{B}\cdot\overleftrightarrow{g}\cdot\vec{S} - g_H\mu_N\vec{B}\cdot\overleftrightarrow{I}^{H} + \vec{I}\cdot\overleftrightarrow{A}^{H}\cdot\vec{S} + \vec{I}\cdot\overleftrightarrow{A}^{Cu}\cdot\vec{S} + \vec{I}\cdot\overleftrightarrow{P}^{Cu}\cdot\vec{I} - g_{Cu}\mu_N\vec{B}\cdot\vec{I}^{Cu} \quad (2)$$

the proton–proton dipolar coupling is neglected. The maximum splitting for two protons in one methyl group is only 70 kHz. Therefore, these splittings can be observed only in some directions of the magnetic field (see Figure 7), thus making a precise determination of the tensor impossible. On the other hand, however, the splitting of the H(10-2N) proton can be used to assign three protons to one methyl group. In the analysis of the ENDOR data, the average of the three frequencies was used. The data were again treated with the computer program ESR64. In this application, the error function (1) was minimised by varying the elements of the proton hyperfine coupling tensor. Because of the complexity of the spectra, only four tensors could be determined. They are listed in Table 6. An indication of the accuracy of the tensors is the error function (1): it ranges from 0.0009 to 0.027 × 10^{-4} cm^{-1} for these four tensors. The assignment to the correct protons and the analysis of another five tensors was possible only by elaborate computer calculations as described earlier.[25] In this method, the coefficients of the molecular orbital of the unpaired electron (as obtained from the EHMO calculation) are used to calculate the hyperfine coupling tensors, *including the two- and three-centre contributions.* From these theoretical tensors, the predicted ENDOR frequencies are calculated and compared with the experimental frequencies. In this way, the four tensors in Table 6 could be assigned to one *intra*molecular proton [H(2)] and three protons of neighbouring molecules [attached to C(9), C(10), and C(11)]. The signs of the principal values cannot be determined with ENDOR. For the intermolecular protons they are given the signs of the calculated tensors which results in positive isotropic couplings, indicating a positive spin density. The correspondence between the experimental and the calculated H(2) tensor is good for the directions but not for the principal values. It is coincident with the copper hyperfine tensor, as expected, but the magnitude is unusual, although A_1 is similar to the value as determined by Kirste and van Willigen[14] for [Cu(pd)$_2$] in frozen solution. The tensor has the format expected for a proton in a π-radical, but clearly this is not the mechanism of spin transfer in this case. Most of the spin density reaches it by direct

Table 6. Experimental and theoretical hyperfine tensors for [Cu(tmhd)$_2$] in [Pd(tmhd)$_2$] and copper–proton distances. Directions are in degrees relative to the molecular axis system

			Experimental				Theoretical			
	Cu–H distance	Hyperfine	Coupling	Directions			Coupling	Directions		
Proton	(Å)	component	(MHz)	*x*	*y*	*z*	(MHz)	*x*	*y*	*z*
H(2)	4.034	A_1	±2.51	95	87	174	−1.15	91	90	179
		A_2	∓0.61	12	102	96	2.04	5	92	91
		A_3	∓1.90	100	160	92	−0.84	89	164	90
		A_{iso}	∓0.29							
H(9-1N)	4.354	A_1	3.85	93	118	30	3.30	96	111	23
		A_2	−1.38	168	94	98	−1.43	124	133	112
		A_3	−2.47	80	146	119	−1.82	35	125	98
		A_{iso}	0.06							
H(10-2N)	2.923	A_1	6.65	79	103	163	5.54	79	106	160
		A_2	−3.11	12	91	79	−2.41	124	140	83
		A_3	−3.54	91	159	77	−2.91	143	59	108
		A_{iso}	0.35							
H(11-1N)	4.389	A_1	4.15	88	124	36	3.61	64	92	27
		A_2	−1.90	147	113	107	−1.60	71	28	98
		A_3	−2.26	58	132	121	−1.87	146	68	65
		A_{iso}	0.22							

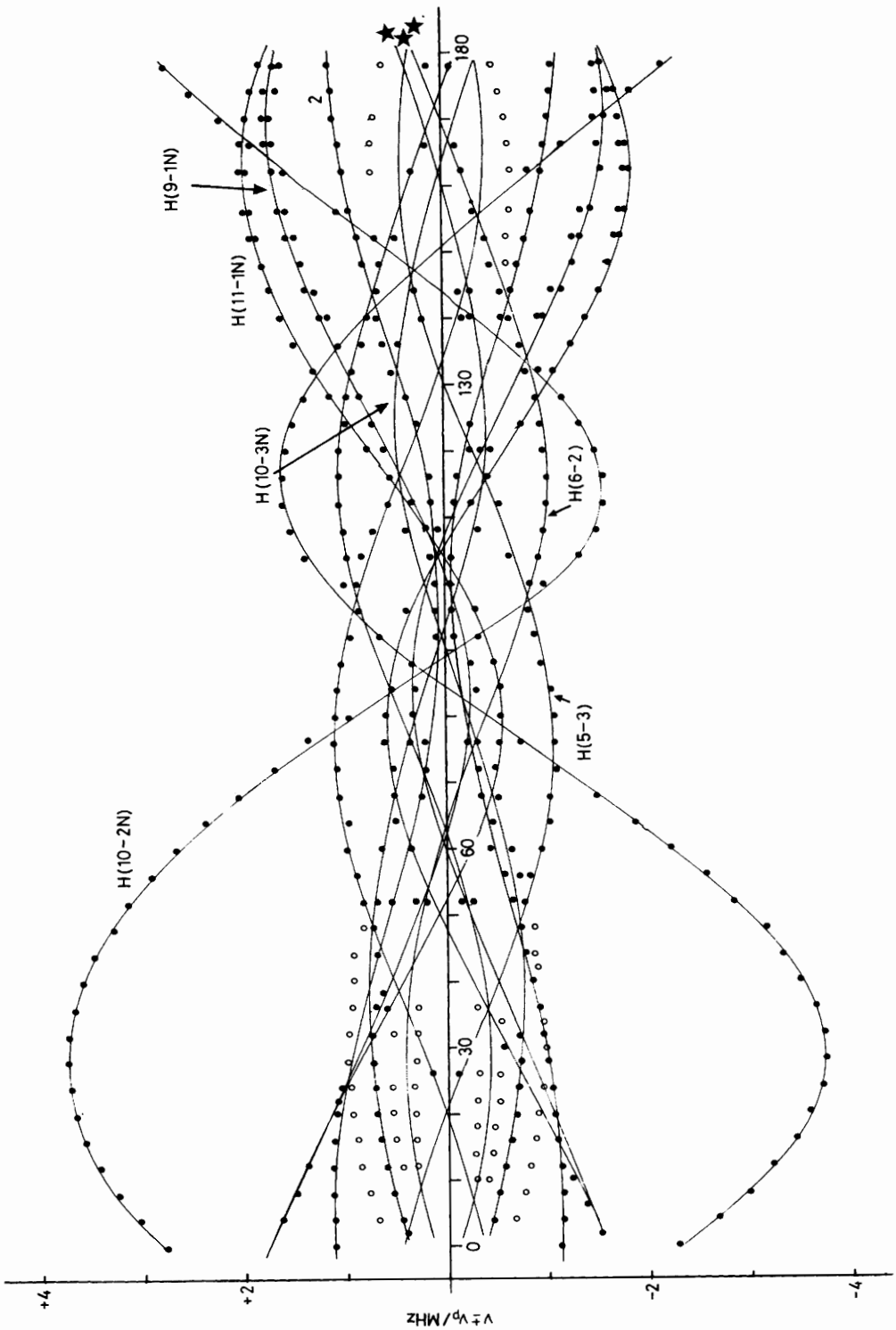

Figure 7. Angular variation of the proton ENDOR spectrum of $[Cu,Pd(tmhd)_2]$. The points (●) are the experimental data and the curves are those fitted to the data by the minimisation routines, except those marked (★) which are theoretical curves from the EHMO calculations that fit the remaining data well. The circles (○) are data points that could not be fitted either by the minimisation routine or by the theoretical angular variations produced by the EHMO calculations

Table 7. Theoretical tensors for $[Cu(tmhd)_2]$ in $[Pd(tmhd)_2]$ and copper–proton distances. Directions are in degrees relative to the molecular axis system

Proton	Cu–H distance (Å)	Hyperfine component	Coupling (MHz)	Directions		
				x	*y*	*z*
H(5-3)	4.215	A_1	1.99	63	141	114
		A_2	−0.95	28	68	81
		A_3	−1.04	87	115	26
H(6-2)	4.276	A_1	1.99	61	144	72
		A_2	−0.92	150	115	83
		A_3	−1.04	87	108	161
H(10-1N)	4.484	A_1	1.79	63	108	147
		A_2	−0.28	56	129	58
		A_3	−1.37	133	131	97
H(10-3N)	5.513	A_1	1.51	80	116	151
		A_2	−0.67	126	134	74
		A_3	−0.78	142	61	113
H(11-2N)	4.442	A_1	1.88	109	148	73
		A_2	−0.98	143	82	126
		A_3	−1.09	61	116	140

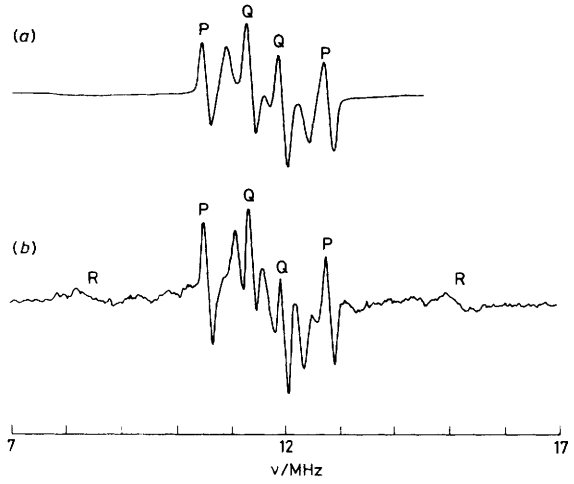

Figure 8. Proton ENDOR spectra taken on the Cu $M_I = +\frac{3}{2}$ (∥) line: (*a*) frozen solution at 77 K, (*b*) powdered dilute crystal

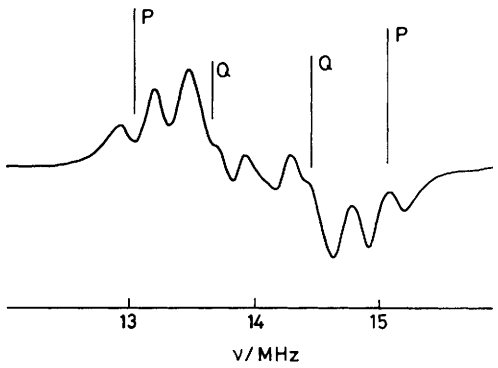

Figure 9. Proton ENDOR spectrum taken on the Cu $M_I = -\frac{1}{2}$ (⊥) line for a frozen solution of $[Cu(tmhd)_2]$ in CH_2Cl_2–toluene at 77 K

delocalisation. In addition, there are dipolar interactions. However, there must be polarisation of electrons in the π-ring system which in turn can contribute to this tensor, as well as mixing in of excited-state ($d_{xz,yz}$) orbitals which can genuinely provide a mechanism for π-delocalisation. Separating these contributions would be very difficult. A determination of the sign of this coupling with triple resonance could give more information about the mechanism of spin transfer to this proton.

The theoretical tensors of the other five protons that can be fitted are listed in Table 7. Only two of them [H(5-3) and H(6-2)] are *intra*molecular protons. These are the two protons within the molecule that are closest to the central atom, 4.215 and 4.276 Å respectively from the copper. The corresponding protons in the other Bu^t group, attached to C(9)—C(11), do not seem to fit the data in any way. It is this group that has the disorder and the positions used to calculate the tensors are the same as were used successfully to match the variation of the interaction with the four external protons H(9-1N), H(10-2N), H(10-3N), and H(11-1N). This could suggest that the Bu^t group on C(3) in the molecules containing a copper atom is in one of the disorder positions, but in those molecules containing the palladium host atom in different disorder positions. Although the energy barriers involved must be small, it may be doubted, however, whether the doping with copper can affect the preferred conformation. There were other families of lines which were observed at only a few angles but there were insufficient data to assign them. These are represented by open circles in Figure 7.

Frozen Solution and Powder ENDOR.—The spectrum of powdered crystals of $[Cu,Pd(tmhd)_2]$ and of a frozen solution of $[Cu(tmhd)_2]$ in CH_2Cl_2–toluene are shown in Figures 8 and 9. The spectra were recorded on the Cu $M_I = +\frac{3}{2}$ (∥) e.s.r. line (Figure 8) and on the Cu $M_I = -\frac{1}{2}$ (⊥) e.s.r. line (Figure 9). The spectra in Figure 8 are 'single-crystal like' and the hyperfine couplings observed should directly relate to proton couplings along the *z* axis in the single crystal. (These are not proton principal values because most proton tensors are not parallel with the molecular axis system.)

The spectra of powdered crystals and of the frozen solution are quite different, although two pairs of lines in each are coincident. The coincident lines must arise from intramolecular protons, whilst the extra lines in the powdered crystals must arise from intermolecular protons. The large coupling of 6.43 MHz (R) in Figure 8(*b*), not seen in Figure 8(*a*), is very close to

the principal value ($A_1 + A_{iso}$) of proton H(10-2N) (7.00 MHz) which is the next nearest proton on the adjacent molecule. Coincident proton couplings occur at 2.14 and 2.19 MHz (P) and 0.55 and 0.52 MHz (Q) for solution and powdered crystal respectively. The latter must arise from Bu^t protons, but a firm assignment cannot be made. However, the former match almost exactly the principal value ($A_1 + A_{iso}$) of 2.194 MHz, which lies parallel to the z axis as deduced from the single-crystal data.

The ENDOR spectrum taken on a Cu perpendicular line (Figure 9) is much more difficult to interpret because of the complicated angular variation and splitting of the lines. However, since one of the principal values of the H(2) proton lies along the x axis, it would be expected that a corresponding hyperfine coupling would be clearly seen in the powder ENDOR spectrum on $g_\perp$. A pair of lines separated by 2.1 MHz (P) (Figure 9) in the frozen solution almost exactly matches the principal value ($A_3 + A_{iso}$) of 2.217 MHz deduced from the single crystal, and another pair of 0.8 MHz (Q) likewise matches the principal value ($A_2 + A_{iso}$) of 0.896 MHz.

Conclusions

The analysis of proton hyperfine couplings in the ENDOR spectra of copper complexes having many protons in their ligands is difficult even when single crystals are used. It is, however, possible with elaborate computer calculations. In contrast, much information is lost if frozen solutions are used although a number of proton ENDOR lines may be observed. Even if ENDOR spectra are recorded on an extreme parallel feature, few of the protons will have a principal direction coincident with the same axis. Many frozen-solution ENDOR lines can be assigned with the knowledge of a single-crystal analysis.

Acknowledgements

We thank the Royal Society and the S.E.R.C. for research grants and the S.E.R.C. for a studentship (G. J. B.).

References

1 A. N. Knyazeva, E. A. Shugam, and L. M. Shkol'nikova, *Zh. Strukt. Khim.*, 1970, **11**, 938.
2 G. D. Fallon and B. M. Gatehouse, *Cryst. Struct. Commun.*, 1982, **11**, 1317.
3 S. Okeya, S. Ooi, K. Matsumoto, Y. Nakamura, and S. Kawaguchi, *Bull. Chem. Soc. Jpn.*, 1981, **54**, 1085.
4 S. H. Simonson, W. Y. Hsiang, and D. M. Normand, *Am. Crystallogr. Assoc., Ser. 2*, 1978, **6**, 14.
5 H. Koyama, Y. Saito, and H. Kuroya, *J. Inst. Polytech. Osaka City Univ. Ser. C*, 1953, **4**, 43.
6 P. K. Hon, C. E. Pfluzer, and R. L. Belford, *Inorg. Chem.*, 1966, **5**, 516.
7 M. Blackstone, J. van Thuijl, and C. Romers, *Recl. Trav. Chim. Pays-Bas*, 1966, **85**, 557; A. N. Knyazeva, E. A. Shugam, and L. M. Shkol'nikova, *Zh. Struct. Khim.*, 1969, **10**, 83.
8 F. A. Cotton and J. J. Wise, *Inorg. Chem.*, 1966, **5**, 1200.
9 A. H. Maki and B. R. McGarvey, *J. Chem. Phys.*, 1958, **29**, 31.
10 S. Kita, M. Hashimoto, and M. Iwaizumi, *J. Magn. Reson.*, 1982, **46**, 361.
11 H. So and R. L. Belford, *J. Am. Chem. Soc.*, 1969, **91**, 2392.
12 F. A. Cotton and J. J. Wise, *Inorg. Chem.*, 1967, **6**, 915.
13 F. A. Cotton, C. B. Harris, and J. J. Wise, *Inorg. Chem.*, 1967, **6**, 909.
14 B. Kirste and H. van Willigen, *J. Phys. Chem.*, 1983, **87**, 781.
15 D. Snaathorst, C. P. Keijzers, A. A. K. Klaassen, E. de Boer, V. P. Chacko, and R. Gomperts, *Mol. Phys.*, 1980, **40**, 585.
16 M. S. Lehman and F. K. Larsen, *Acta Crystallogr., Sect. A*, 1974, **30**, 580.
17 D. F. Grant and E. J. Gabe, *J. Appl. Crystallogr.*, 1978, **11**, 114.
18 A. C. T. North, D. C. Philips, and F. S. Mathews, *Acta Crystallogr., Sect. A*, 1968, **24**, 351.
19 P. T. Beurskens, W. P. Bosman, H. M. Doesburg, Th. E. M. Van den Hark, P. A. J. Prick, J. H. Noordik, G. Beurskens, R. O. Gould, and V. Parthasarathi, in 'Conformation in Biology,' eds. R. Srinivasan and R. H. Sarma, Adenine Press, New York, 389.
20 G. M. Sheldrick, SHELX, program for crystal structure determination, University Chemical Laboratory, Cambridge, 1976.
21 N. Walker and D. Stuart, *Acta Crystallogr., Sect. A*, 1983, **39**, 158.
22 'International Tables for *X*-Ray Crystallography,' Kynoch Press, Birmingham, 1974, vol. 4.
23 J. Stach, R. Kirmse, U. Abram, W. Dietzsch, J. H. Noordik, K. Spee, and C. P. Keijzers, *Polyhedron*, 1984, **3**, 433.
24 L. D. Rollman and S. I. Chan, *J. Chem. Phys.*, 1969, **50**, 3416.
25 C. P. Keijzers and D. Snaathorst, *Chem. Phys. Lett.*, 1980, **69**, 348.

Received 11*th November* 1985; *Paper* 5/1975